




## Article

# The Impact of Thermal Inertia on the Indoor Thermal Environment of Light Steel Framing Constructions

Eduardo Roque <sup>1,\*</sup>, Romeu Vicente <sup>1,\*</sup>, Ricardo M. S. F. Almeida <sup>2,3</sup> and Victor M. Ferreira <sup>1</sup>

<sup>1</sup> RISCO—Risks and Sustainability in Construction, Department of Civil Engineering, University of Aveiro, 3810-193 Aveiro, Portugal; eroque@ua.pt (E.R.); victorf@ua.pt (V.M.F.)

<sup>2</sup> Department of Civil Engineering, Polytechnic Institute of Viseu, School of Technology and Management, Campus Politécnico de Repeses, 3504-510 Viseu, Portugal; ralmeida@estgv.ipv.pt

<sup>3</sup> CONSTRUCT-LFC, Faculty of Engineering (FEUP), University of Porto, Rua Dr. Roberto Frias s/n, 4200-465 Porto, Portugal

\* Correspondence: romvic@ua.pt

**Abstract:** Typically, reinforced concrete and brick masonry construction is the most common construction system of the majority of the southern European residential building stock. However, the lightweight steel framing (LSF) construction system has been progressively assuming a relevant position in the residential sector. Since LSF is not the traditional construction system, the indoor thermal environment of these buildings has not been widely studied and discussed considering the southern European climate context. The low thermal inertia of this construction system is commonly pointed to as a possible weakness in warmer climates. The present work aims to address this research gap by evaluating and comparing the LSF and masonry construction systems in terms of the indoor thermal environment focusing on the level of thermal inertia. The considered methodology lies in a long-term experimental campaign based on the construction and monitoring of two identical experimental test cells, differing only in the construction system. The test cells are in the central region of Portugal. The monitoring period elapsed over an entire year. Dynamic simulations are also carried out with a model experimentally validated to consider a wider range of climatic conditions. It is shown that internally insulating the ground floor has an impact on the indoor thermal environment of the LSF test cell by accentuating the indoor air temperature fluctuations and magnitude of the extreme peak values. However, the results also reveal that the faster and closer response to the outdoor conditions may be beneficial for LSF buildings during the heating season.

**Keywords:** light steel framing; masonry; indoor thermal environment; southern European; thermal inertia



**Citation:** Roque, E.; Vicente, R.; Almeida, R.M.S.F.; Ferreira, V.M. The Impact of Thermal Inertia on the Indoor Thermal Environment of Light Steel Framing Constructions. *Energies* **2022**, *15*, 3061. <https://doi.org/10.3390/en15093061>

Academic Editors: Catarina Serra and Nuno Simões

Received: 11 February 2022

Accepted: 20 April 2022

Published: 22 April 2022

**Publisher's Note:** MDPI stays neutral with regard to jurisdictional claims in published maps and institutional affiliations.



**Copyright:** © 2022 by the authors. Licensee MDPI, Basel, Switzerland. This article is an open access article distributed under the terms and conditions of the Creative Commons Attribution (CC BY) license (<https://creativecommons.org/licenses/by/4.0/>).

## 1. Introduction

Nowadays, millions of Europeans remain indoors about 90% of their time, and it is estimated that the majority of this time is spent at home [1]. Therefore, designing buildings that can achieve proper levels of indoor thermal comfort for their occupants must be seen as a core requirement. The impact of the indoor thermal environment on the occupants has been a research line addressed by several authors. It is acknowledged that the quality of the indoor thermal environment has a significant influence at several levels, including human mental state [2,3], work productivity [4,5], health [6,7], and also energy consumption [8,9].

Southern European climates are characterised by their strong dynamic character, which is translated into considerable seasonal and daily temperature variations. During the cooling season, high outdoor temperatures coupled with strong solar radiation may raise overheating concerns during the warmer periods of the day, followed by potential cooling during the night. During the heating season, the external weather is milder than in colder central and northern European climates, however, with marked differences from the summer period. Therefore, the southern European residential construction coupled

with these climatic characteristics translate into construction features aiming to buffer the variability of the external weather and therefore contribute to achieving a more stable and comfortable indoor thermal environment.

Constructing buildings with high thermal inertia using solid and dense materials is characteristic of the southern European architecture [10]. This vernacular feature is associated with effective passive strategies allowing for enhancing the indoor thermal comfort of buildings by providing a buffering capacity against the outdoor conditions [11,12], especially in southern European climates, where there are substantial daily and seasonal outdoor dry-bulb temperature fluctuations and significant maximum peak temperatures during the summer [13–15]. Thermal inertia is also a relevant factor in buildings with high internal gains, being a passive measure to control overheating problems

Buildings with high thermal inertia are able to provide some inertia against outdoor temperature stimulus and, therefore, time shift and flatten out temperature fluctuations. Therefore, thermal inertia can be used to absorb heat gains during the day and release the stored energy during the night period. When combined with suitable bioclimatic design and efficient use of the solar gains, the thermal inertia of the building can be effectively used to improve the indoor thermal comfort passively and consequently decrease the energy consumption.

On the other hand, during the winter, high levels of thermal inertia can have adverse effects. Buildings can present a slower response to the heating systems and therefore consume more energy and take more time to reach the indoor comfort conditions [12], which is particularly relevant considering the intermittent heating patterns common in the southern European building context [16].

Nowadays, the heavyweight reinforced concrete and brick masonry construction system is the most conventional in southern European countries.

Nevertheless, over the past years, there has been a progressive shift to more industrialised alternatives that have been gaining more relevance and visibility, such as the Light Steel Framing (LSF) construction system. Unlike the common heavier buildings, LSF constructions are usually characterised by their low thermal inertia due to the low mass and reduced thickness of the materials used in this construction. Therefore, it is widely referenced in the literature that the risk of overheating and significant indoor temperature fluctuations in lightweight buildings located in warmer climates is a big challenge that must be addressed [13,15,17–19].

LSF buildings present the capacity to address some of the major concerns of the construction sector, offering valuable opportunities in terms of sustainability and construction efficiency, with advantages over the more common and established construction systems [20,21]. Advantages such as the speed of construction, the reduced necessity for on-site space, lower necessity of the workforce, high factory quality control, lower water consumption, reduced construction and demolition waste, recovery, and recyclability potential of the used materials [22–24] are important advantages towards the EU's goals for promoting the decarbonisation of the construction sector. Additionally, LSF buildings can provide a prime alternative in terms of providing housing or shelter in remote regions or in crises [25].

However, since LSF is not the traditional or most common construction system, the indoor thermal environment of these buildings has not been broadly characterised considering the southern European climate context. There is a lack of experimental research work oriented to the study of LSF buildings and the comparison with the common brick masonry and reinforced concrete buildings. The scarcity of widespread and consolidated information concerning the thermal behaviour of LSF buildings in this climate context constrains its sustained proliferation.

Herein, this research study aims to address this gap by evaluating and comparing the indoor thermal environment of the LSF and masonry construction systems. A long-term experimental campaign was carried out based on the construction and monitoring of two

experimental test cells, differing exclusively in the construction system. The test cells are located in the central region of Portugal and were monitored for an entire year.

The experimental campaign encompasses two stages. In the first stage, the test cells are analysed and compared, considering a baseline constructive scenario. In this scenario, both test cells count with the contribution of the uninsulated concrete ground floor slab for thermal inertia. In the LSF test cell, this element is the most important contributor to the overall thermal mass, contrasting with the walls and roof assemblies. The second stage involves assessing the impact of reducing the thermal inertia of the test cells by internally insulating the ground floor slab.

The results of the experimental campaign are further complemented in a second phase by computational analysis resorting to dynamic simulation, aiming to extend the research scope to different climatic conditions and consequently assess the degree of dependence of the obtained conclusions on the outdoor conditions.

Dynamic simulation of buildings constitutes an important tool to reliably assess buildings holistically and computationally characterise the indoor thermal environment of a building rigorously and reliably. Computer simulations are currently widely used in the construction sector as they can provide a cost-effective and time-efficient solution to conduct parametric analyses considering different factors affecting the indoor thermal environment and their impact. Furthermore, computational simulations assume an added layer of robustness when linked with experimental results that can validate the models and further support additional analysis [26,27].

## 2. Case Study and Experimental Methodology

### 2.1. Experimental Approach

The experimental campaign comprises the monitoring of two similar test cells: one was built according to the reinforced concrete and hollow brick masonry construction system (HBM test cell) and the other according to the LSF construction system (LSF test cell). The test cells are located in Albergaria-a-Velha, in the Aveiro District (central coast region of Portugal, Csb climate, according to the Köppen-Geiger classification).

The geometry and volumetry of the test cells are aligned with a real building compartment, presenting inner floor dimensions of 3.87 m by 2.97 m and a height of 2.70 m, which totalises an interior volume of approximately 31 m<sup>3</sup>. The test cells have their longitudinal axis roughly along the north-south (155° SE) direction.

The walls and roof of both test cells present the same thermal transmittance (U-value). Nevertheless, these elements are characterised by very different dynamic thermal parameters, which translate to the differences in terms of thermal inertia between the two test cells. The LSF walls and roof reveal a much lower internal areal heat capacity ( $k_1$ ) value, implying a minor ability of the most inner layers of the opaque elements to store and release heat when the indoor temperature varies periodically. Furthermore, the LSF elements present a higher decrement factor ( $f$ ), indicating a lower ability to delay the outgoing or incoming thermal wave across the building's opaque fabric. Detailed information regarding the constructive configuration of the test cells can be found in [16,28,29].

The experimental campaign was maintained for one year, from October 2019 to September 2020, and two setups were sequentially monitored: (a) insulated case; (b) uninsulated case.

Figure 1a introduces a plan view and vertical cross section of the test cells, indicating, schematically, the position of the thermal insulation over the ground floor and of the different sensors used for monitoring the indoor air temperature. For the scenario of the insulated ground slab, the entire area was completely covered with 5 cm thick expanded polystyrene boards ( $\lambda = 0.036 \text{ W}\cdot\text{m}^{-1}\cdot\text{°C}^{-1}$ ). Pictures of the thermal insulation are shown in Figure 1b.

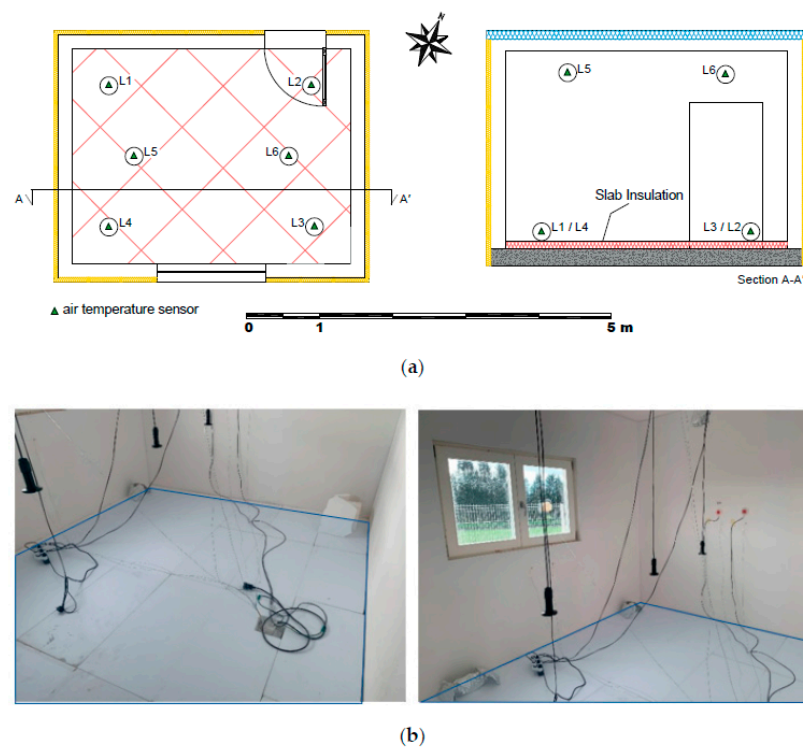


**Figure 1.** Experimental test cells (Setup 1): (a) plan view and section A-A' indicating the monitoring positions; (b) expanded polystyrene boards completely covering the ground slab.

## 2.2. Dynamic Simulation

In order to also assess the indoor thermal environment of the LSF buildings and the impact of insulating the ground slab considering different climatic conditions, a computational model of the LSF test cell was developed using DesignBuilder software [30]. A preview of the developed geometric model of the LSF test cell can be seen in Figure 2.

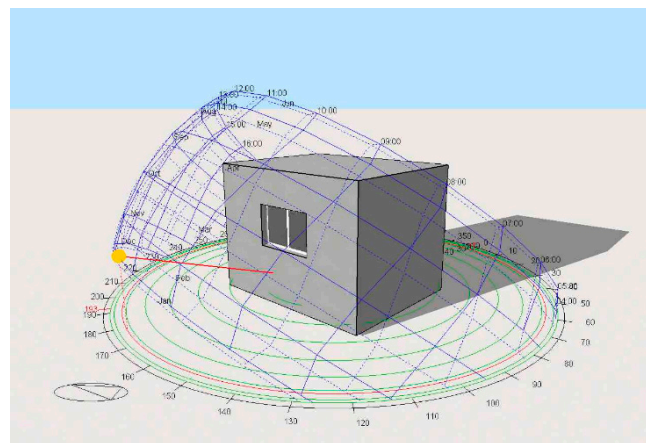


**Figure 2.** The geometric model of the LSF test cell considered in the dynamic simulations.

The results obtained from the dynamic simulation were verified against the experimental data in terms of indoor air temperatures over the entire year. At the end of the process, the overall goodness-of-fit (*GOF*) index is computed to assess and classify the accuracy of the model. The *GOF* index is calculated using the normalized mean bias error (*NBME*), and the coefficient of variation of the root mean square error (*CVRMSE*). These indexes are calculated according to the following equations, where  $M_i$  and  $S_i$  represent

measured and simulated data points for each time instance  $i$  (hourly values) and  $n$  is the total number of data points for the considered period.

$$GOF (\%) = \frac{\sqrt{2}}{2} * \sqrt{NMBE^2 + CVRMSE^2} \quad (1)$$

$$NMBE = \frac{\sum_{i=1}^n (M_i - S_i)}{n * \bar{M}_i} * 100 \quad (2)$$

$$CVRMSE = \frac{\sqrt{\frac{1}{n} * \sum_{i=1}^n (M_i - S_i)^2}}{\bar{M}_i} * 100 \quad (3)$$

A  $GOF$  value of 4.4% was calculated following the methodology above. In Figure 3, the relationship between the measured and simulated indoor air temperature in the LSF test cell is presented for the entire monitored period, together with the respective coefficient of determination ( $R^2$ ). The calculated  $R^2$  value assumes a significant order of magnitude, indicating a good accuracy of the dynamic model, which is also supported by the  $GOF$  value.

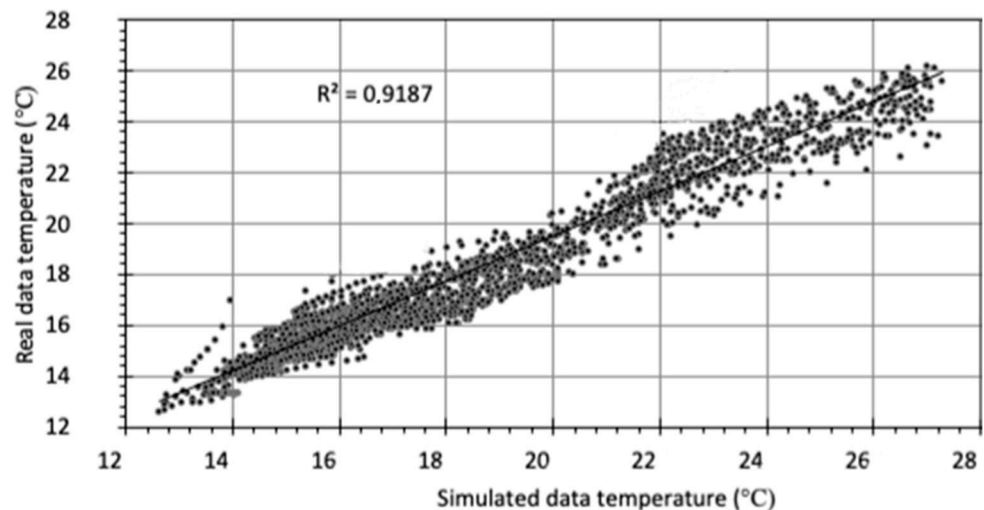


**Figure 3.** Relationship between the measured and simulated indoor air temperature in the LSF test cell for the entire monitored period.

The methodology for the dynamic simulations encloses the assessment of the indoor thermal environment of the LSF test cell considering five additional climates, characterising distinct climatic conditions in Portugal. The cities of Aveiro, Bragança, Évora, Faro, and Lisboa, represented in Figure 4, were selected to cover a wide array of profiles in terms of outdoor dry-bulb temperatures fluctuation and peak values.

Table 1 presents relevant climatic data from these locations [31,32], namely the duration of the heating season ( $M$ ), the average heating season outdoor dry-bulb temperature ( $\Theta_{ext,h}$ ), the minimum heating season outdoor dry-bulb temperature ( $\Theta_{ext,min}$ ), the heating degree-days ( $GD$ ), the average cooling season outdoor dry-bulb temperature ( $\Theta_{ext,c}$ ), the maximum cooling season outdoor dry-bulb temperature ( $\Theta_{ext,max}$ ), and the average monthly value of solar radiation incident on a south-oriented vertical surface ( $G_{South}$ ).





**Figure 4.** Location of the cities considered in the dynamic simulations within the Portuguese territory.

**Table 1.** External weather characteristics of the climates considered in the dynamic simulations.

	Aveiro	Bragança	Évora	Faro	Lisboa
M [months]	6.3	7.3	5.3	4.8	5.3
$\Theta_{\text{ext,c}}$ [°C]	9.5	5.5	10.0	11.3	10.8
$\Theta_{\text{ext,min}}$ [°C]	0.9	−2.3	1.6	3.3	3.7
GD [°C]	1337	2015	1150	987	1071
$\Theta_{\text{ext,h}}$ [°C]	20.6	21.5	24.3	23.1	21.7
$\Theta_{\text{ext,max}}$ [°C]	32.3	35.9	39.1	35.0	32.1
$G_{\text{South}}$ [kWh/m <sup>2</sup> ]	140	125	150	155	150

### 2.3. Monitoring Equipment

The measurements and monitoring conditions considered in the present work were carried out according to the standard ISO 7726 [33]. All the measured data were collected at 10 min intervals. A data logger and several sensors were considered:

- i. Outdoor environmental conditions (data logger: data collected using two ICP I-7015P input modules and two I-7561 modules):
  - A weather station with the following sensors:
    - Pyranometer LP PYRA03AC, measuring the global horizontal radiation (accuracy:  $\pm 5 \text{ W/m}^2$ );
    - Thermo Hygrometer DeltaOHM HD9007-A1, including a double antiradiation shield (accuracy:  $\pm 0.1 \text{ }^\circ\text{C}$  and  $\pm 2\% \text{ HR}$ ).
- ii. Indoor environmental conditions:
  - Indoor air temperature—SHT31 temperature and relative humidity sensors (accuracy:  $\pm 0.3 \text{ }^\circ\text{C}$  and  $\pm 2\% \text{ HR}$ ) allocated according to the schematic layout presented in Figure 1a. The sensors were distributed among an inferior level (0.1 m from the ground floor slab) and a superior level (2.4 m from the slab).

## 3. Experimental Campaign—Results and Discussion

### 3.1. Indoor Thermal Environment—Representative Summer, Shoulder Season, and Winter Weeks

The characterisation of the indoor thermal environment of the test cells is presented based on the analysis and discussion of the indoor air temperature profiles during representative summer, shoulder season, and winter weeks. All the results presented in this section correspond to the insulated case.

- Representative Summer Week

The week between 17–24 July is considered to discuss the summer season. This period is characterised by strong solar radiation (registering values above  $900 \text{ W}\cdot\text{m}^{-2}$ ), high maximum outdoor dry-bulb temperatures (reaching nearly  $40 \text{ }^\circ\text{C}$ ), and significant daily temperature fluctuations (variations up to nearly  $20 \text{ }^\circ\text{C}$ ) as can be seen in Figure 5a. The marked outdoor dry-bulb temperature fluctuations and magnitude of the daily maximum temperatures enhance the use of thermal mass in buildings by mobilising its dynamic behaviour. The indoor air temperature fluctuation in both test cells during the same week is also presented in Figure 5a. The indoor temperature profile for each test cell corresponds to the average value between monitoring levels (ground slab and ceiling). For each level, the average value of the different sensors was calculated.

The differences between test cells in terms of indoor air temperature increase and decrease rates over a daily cycle are obvious. Figure 5a shows that the indoor thermal environment of the LSF test cell responds noticeably to the increase in the outdoor dry-bulb temperature and solar radiation. In turn, the indoor air temperature profile in the HBM test cell is only slightly influenced by the outdoor stimulus. Besides presenting significantly distinctive behaviours during the diurnal period, it can be seen that the indoor air temperature in each experimental test cell also reveals very different behaviours during the night. Once again, the LSF test cell presents a closer response to the outdoor environmental conditions, leading to a marked nocturnal temperature drop in the indoor air temperature. The stability of the indoor air temperature registered in the HBM test cell is another important point, registering a maximum daily and weekly indoor air temperature amplitude of  $1.36 \text{ }^\circ\text{C}$  and  $2.59 \text{ }^\circ\text{C}$ , respectively. In contrast, the LSF test cell registers a less stable indoor air temperature profile. A maximum daily indoor air temperature amplitude of  $5.82 \text{ }^\circ\text{C}$  and a maximum weekly amplitude of  $10.02 \text{ }^\circ\text{C}$  was measured in this test cell. The biggest difference between experimental test cells is registered on 17 July, the hottest day of the week. On this day, a difference between test cells of approximately  $5 \text{ }^\circ\text{C}$  was registered.

The registered differences between test cells can predominantly be attributed to the higher  $k_1$  value of the HBM test cell, which allows to more effectively damp temperature peaks and enhance daily indoor air temperature stabilisation. On the other hand, in the LSF test cell, the capacity to diffuse and store heat in the inner layers is reduced, leading to a more pronounced indoor temperature buildup during the warmer periods of the day. Furthermore, because of the lower  $f$  value of the walls and roof, the HBM test cell presents an improved capacity to lessen the incoming thermal wave, causing a lower heating rate of the indoor air.

- Representative Shoulder Season Week

The period between 15–22 May is analysed to discuss the shoulder season. In terms of external weather conditions, the selected week presents mild temperatures, ranging from approximately  $8 \text{ }^\circ\text{C}$  to  $23 \text{ }^\circ\text{C}$  and moderate daily fluctuations (up to approximately  $12 \text{ }^\circ\text{C}$ ), as shown in Figure 5b. Two different periods of the shoulder season week can be identified in terms of outdoor environmental conditions. First, the period between 15–18 May and 20–22 May, is characterised by moderate solar radiation (under  $600 \text{ W}\cdot\text{m}^{-2}$ ), predominantly from open sky sunny days, mild outdoor dry-bulb temperatures, and considerable daily fluctuations. On the other hand, the period of 18–20 May is characterised by cloudy diurnal periods with low and intermittent solar radiation and, therefore, a less variable outdoor dry-bulb temperature profile. Regarding the first period, and in the sequence of what was observed for the summer season week, the two test cells evidence perceptible differences in terms of daily temperature amplitude and magnitude of the peak values. Different thermal behaviour is, however, observed in both test cells in the second period as the solar radiation intensity is lower, and the outdoor dry-bulb temperature profile assumes a stationary behaviour. It can be seen in Figure 5b that, during this period, there were very small differences between the two test cells. The absence of significant exterior stimulus, in terms of amplitude and magnitude, does not allow the demonstration of the dynamic behaviour of the thermal mass. In this context, the gap between test cells in terms of  $k_1$  values is not observable. In fact, during this period, both test cells reveal indoor air temperatures close to

the outdoor dry-bulb temperature because of their stationary behaviour. It was measured in the LSF test cell with a maximum daily indoor air temperature amplitude of  $7.19\text{ }^{\circ}\text{C}$  and a maximum weekly amplitude of  $8.24\text{ }^{\circ}\text{C}$ . The HBM test cell presents a more stable daily indoor temperature profile and low variability over the week, registering maximum values of  $5.26\text{ }^{\circ}\text{C}$  and  $8.36\text{ }^{\circ}\text{C}$ , respectively.

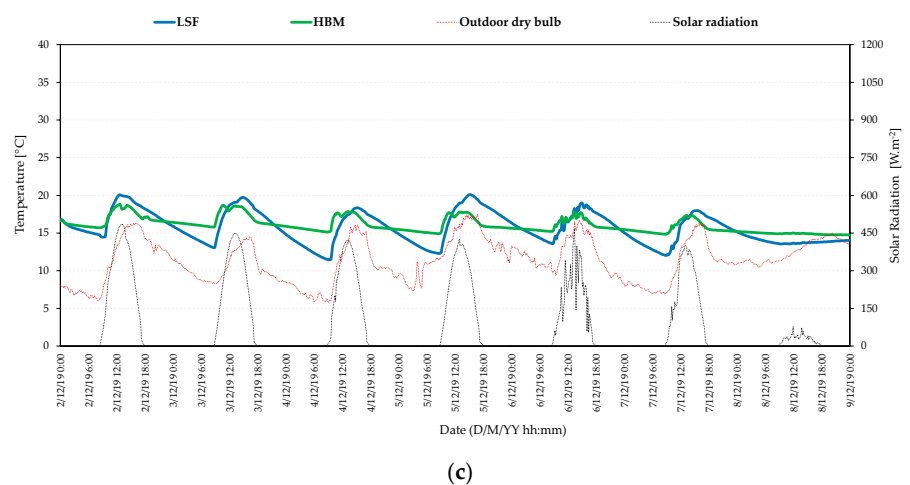
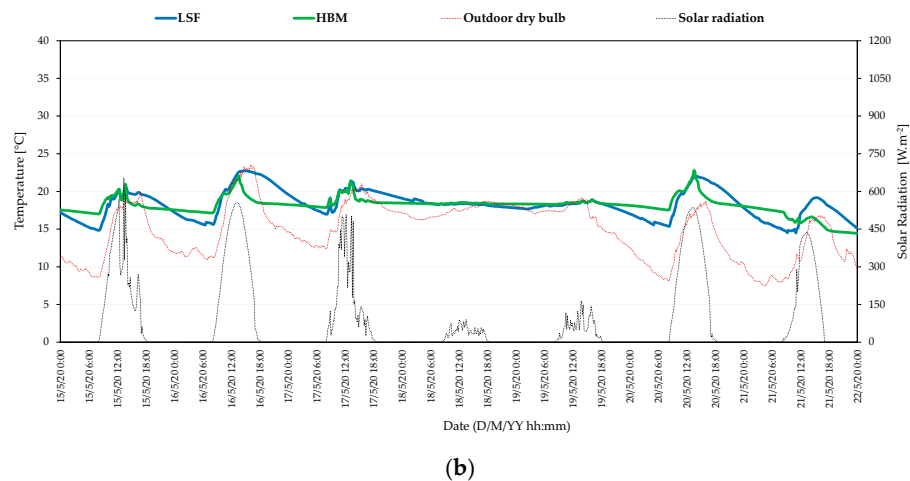
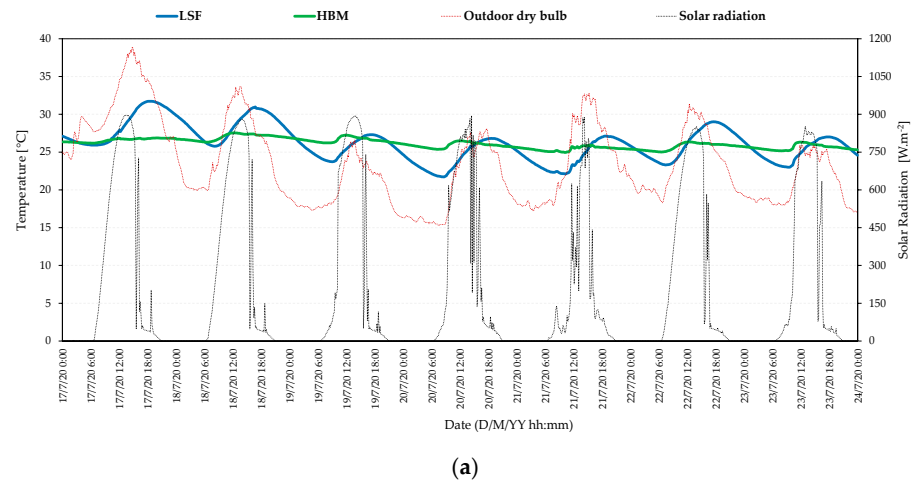


**Figure 5.** Indoor air temperature in the experimental test cells and outdoor environmental conditions during (a) summer week, (b) shoulder season week, and (c) winter week.



- Representative Winter Week

The week from 2 to 9 December was selected to analyse the performance of the test cells during the winter period. This week is characterised by low solar radiation (predominantly under  $450 \text{ W}\cdot\text{m}^{-2}$ ), low outdoor dry-bulb temperatures (minimum values reaching nearly  $5 \text{ }^\circ\text{C}$ ), and modest daily outdoor dry-bulb fluctuations (with variations not exceeding  $10 \text{ }^\circ\text{C}$ ). As shown in Figure 5c and in accordance with previous results, the differences between the indoor air temperature profiles in both test cells are noteworthy. Over the winter week, the LSF test cell measured a maximum daily and weekly indoor air temperature amplitude of  $7.80 \text{ }^\circ\text{C}$  and  $8.65 \text{ }^\circ\text{C}$ , respectively. In its turn, the air temperature in the HBM test cell registers a maximum daily indoor temperature amplitude of  $3.11 \text{ }^\circ\text{C}$  and a maximum weekly amplitude of  $4.04 \text{ }^\circ\text{C}$ . The differences between test cells in terms of minimum indoor air temperature are substantial, especially after the nocturnal temperature drop. During the period between the 15:00 h of 3 December and 09:00 h of 4 December, indoor air temperature drops of approximately  $8.2 \text{ }^\circ\text{C}$  and  $3.0 \text{ }^\circ\text{C}$  were measured in the LSF and HBM test cells, respectively. The maximum difference between cells was registered in the first hours of the morning period on 4 December, when a difference of approximately  $3.70 \text{ }^\circ\text{C}$  was measured.

During the heating season, even in warmer climates such as the southern European, thermally insulating the building envelope is a key requirement in order to reduce heat losses as much as possible. Consequently, the  $f$  value and the U-value of the opaque elements of the external envelope are conventional indicators to assess the performance of buildings during this season. However, it can be concluded from the obtained results that the  $k_1$  value also assumes central importance, leading to a greater stabilisation of the indoor air temperature during a daily cycle due to more efficient management of the solar heat gains.

Figure 6 presents the annual profile of the indoor air temperature registered in each test cell together with the monthly outdoor dry-bulb temperature for the period in which the ground slab was insulated. It can be seen that the indoor air temperature in both test cells is primarily within the higher range of the outdoor dry-bulb temperatures. However, exceptions are registered during the winter months, in which the indoor air temperature exceeds the maximum values measured for the outdoor dry-bulb temperature, showing a greenhouse effect. This situation is more evident in the LSF test cell. This scenario is also registered in the HBM test cell, although in a notable manner only for November and December. In general terms, the small variation of the indoor air temperature can be primarily attributed to the good thermal quality of the external envelope of the test cells and low air permeability, favouring heat conservation. As expected, the results reveal that the differences between test cells are more obvious during months with greater outdoor dry-bulb temperature amplitudes, namely the warmer months of the year.

The interquartile range of the box plots and magnitude of the whiskers is significantly different between the two test cells, showing a predominance of higher indoor air temperatures in the LSF test cell through the monitored period. Differences between indoor air temperature peak values up to nearly  $3.40 \text{ }^\circ\text{C}$  were measured between the test cells. The differences in terms of monthly median value are not so noteworthy, ranging from  $0.05 \text{ }^\circ\text{C}$  to  $1.22 \text{ }^\circ\text{C}$ . The marked influence of the outdoor environmental conditions on the LSF indoor thermal environment is obvious as the outdoor dry-bulb temperature ranges from  $5.80 \text{ }^\circ\text{C}$  to  $38.90 \text{ }^\circ\text{C}$ . The LSF and HBM test cells present an indoor air temperature interval ranging from  $10.59 \text{ }^\circ\text{C}$  to  $31.55 \text{ }^\circ\text{C}$  and from  $13.23 \text{ }^\circ\text{C}$  to  $28.23 \text{ }^\circ\text{C}$ , respectively. The amplitude of the monthly box plots is between  $7.91 \text{ }^\circ\text{C}$  to  $23.59 \text{ }^\circ\text{C}$ . In terms of the indoor thermal environment, the amplitude of the monthly box plots over the monitored period fluctuates from  $7.45 \text{ }^\circ\text{C}$  to  $10.08 \text{ }^\circ\text{C}$  in the LSF test cell and from  $2.41 \text{ }^\circ\text{C}$  to  $5.78 \text{ }^\circ\text{C}$  in the HBM test cell.

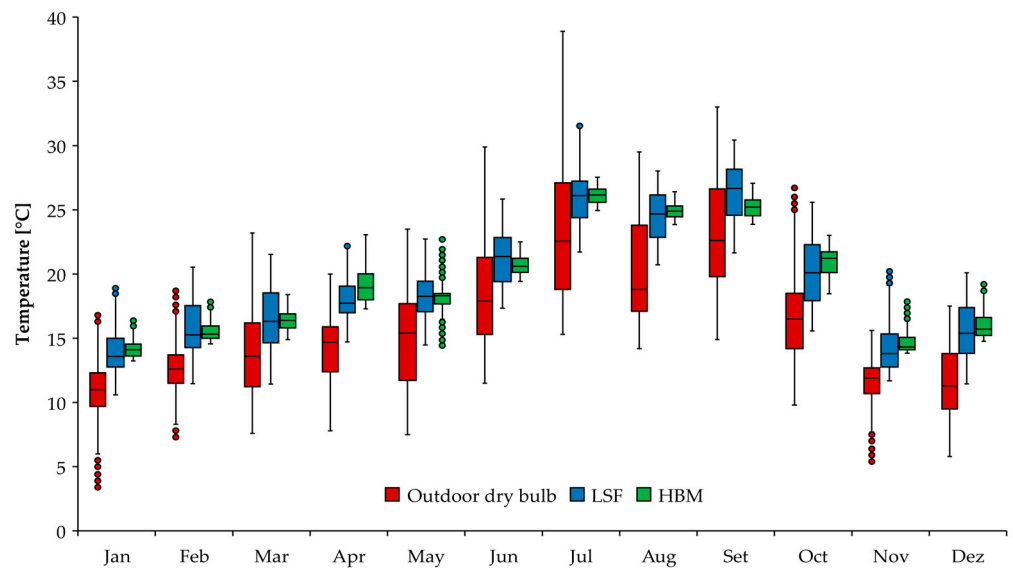


**Figure 6.** Monthly box plot representation of the indoor air temperature and outdoor dry-bulb temperature.

### 3.2. The Importance of the Ground Slab Insulation—Comparison with the Uninsulated Conditions

To initiate the discussion on the comparison between the indoor thermal environment of both test cells when the ground slab is uninsulated and insulated, Figure 7 presents the annual box plot representations of the indoor air temperature considering these scenarios. It is evident that insulating the ground slab impacts the indoor thermal environment of both test cells. The higher median value, superior dimension of the interquartile range, and more expressive values of the maximum and minimum indoor air temperatures confirm that the application of the insulation layer triggers a higher variability of the indoor thermal conditions. It shall be noticed that the impact of not allowing the thermal mass of the ground slab to be effectively mobilised has a higher impact on the LSF test cell. Another important aspect is that the effect of insulating the ground slab is considerably more relevant for the peak values and amplitude of the interquartile range than in terms of median values.

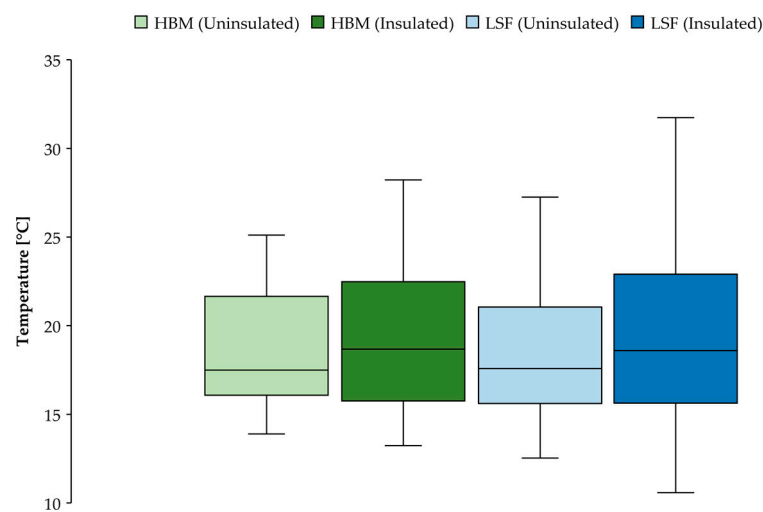


**Figure 7.** Annual box plot representation of the indoor temperature obtained experimentally: uninsulated vs insulated ground slab.

Figure 8 presents the monthly median values of the indoor air temperature of both test cells for the uninsulated and insulated experimental setups. This figure confirms that an

analysis based on median values does not truly translate the existing differences between test cells as the values obtained from the uninsulated configuration almost seamlessly overlap for the two test cells.

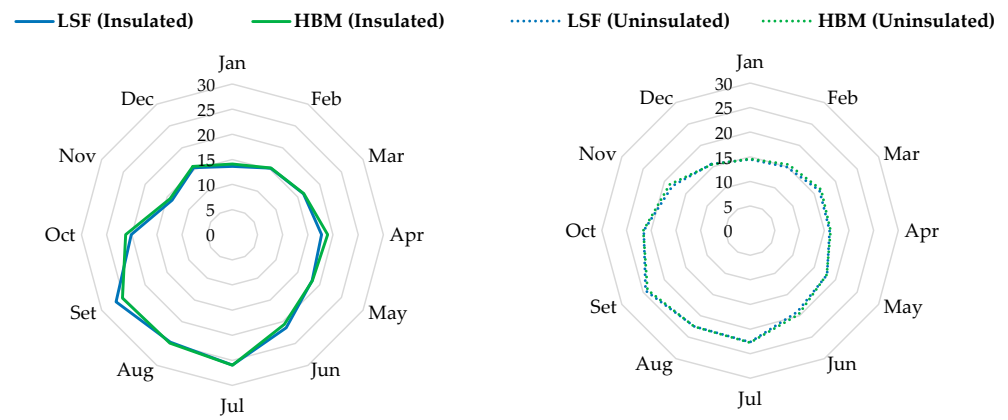


**Figure 8.** Monthly median indoor air temperature for the insulated and uninsulated experimental setups (°C).

The annual profiles obtained for the insulated and uninsulated experimental setups are compared in Figure 9. In this figure, the monthly amplitude of the interquartile range is presented. The amplitude of the interquartile range was considered over the amplitude of maximum and minimum peak values to base this analysis on a more consistent range of indoor air temperatures that more realistically reflects the behaviour over the monitoring period and to minimise the risk of biased conclusions due to the possible impact of outliers. The impact of insulating the ground slab on the indoor thermal environment of the test cells can be clearly identified in Figure 9. The average annual amplitude value for the insulated setup concerning the LSF test cell is 3.14 °C, which contrasts with the average value of 1.69 °C for the uninsulated configuration. On the other hand, insulating the ground slab of the HBM test cell had a much lower effect on the indoor air temperatures. The difference in terms of average annual amplitude value between the insulated and uninsulated configuration is 0.32 °C.

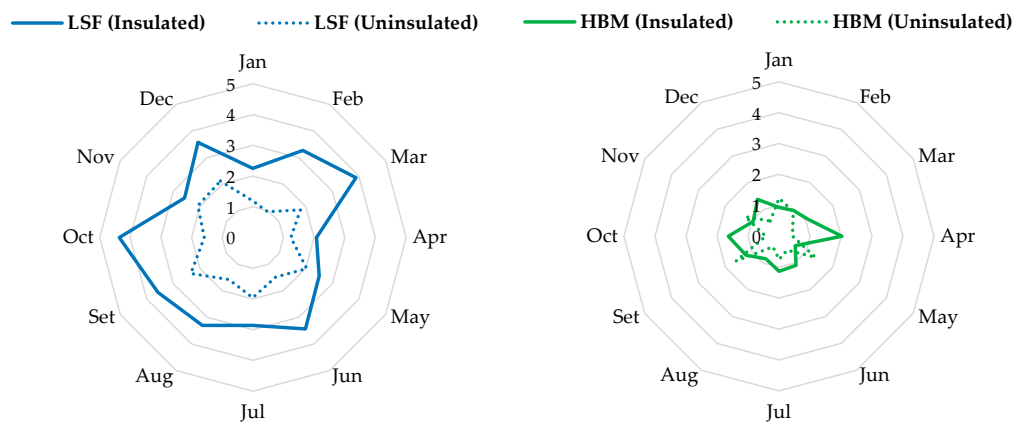


**Figure 9.** Monthly indoor air temperature amplitude for the insulated and uninsulated experimental setups (°C).

#### 4. Dynamic Simulations—Results and Discussion

This section presents and discusses the results concerning the assessment of insulating the ground slab resorting to dynamic simulation. In order to complement and allow an easier comparison with the experimental results, the obtained data are also presented, resorting to annual box plot representations of the indoor air temperature and in terms of annual profiles obtained for the insulated and uninsulated setups.

Figure 10 presents the annual box plot representations of the indoor air temperature considering the five different city locations.

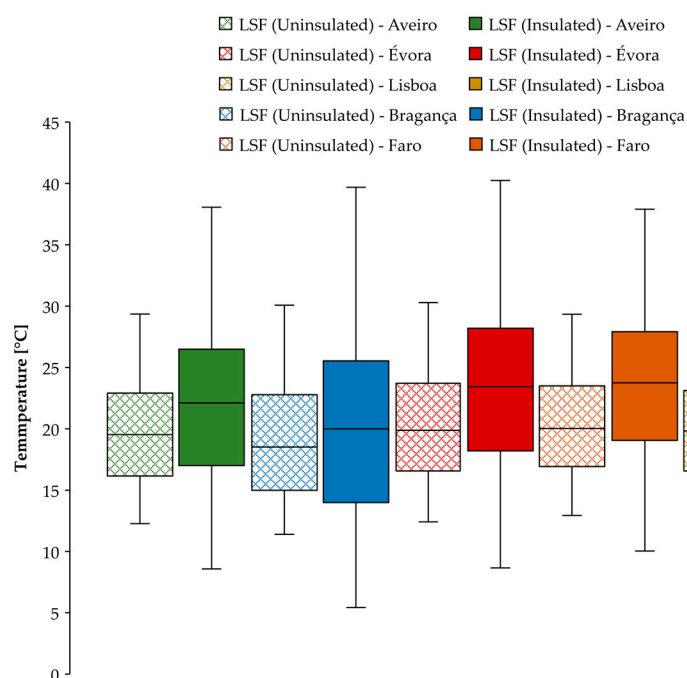


**Figure 10.** Annual box plot representation of the indoor temperature obtained from dynamic simulations: uninsulated vs. insulated ground slab.

The first aspect highlighted in this macroscopic approach is the validation of the substantial impact of insulating the ground slab, regardless of the considered climate. The impact of substantially reducing the thermal inertia of the LSF test cell is more evident during the warmer periods of the year than during the heating season, as shown by the magnitude of the maximum indoor air temperature values and in line with the experimental results. Therefore, climates with more demanding cooling seasons, such as Bragança and Évora, present extremely high maximum indoor temperature peak values exceeding 40 °C. It is therefore shown that thermal inertia is a central feature that must be considered during the design stage, especially in climates with warmer cooling seasons. Otherwise, the risk of overheating and severe discomfort during the summer is substantial.

The impact of reducing the thermal inertia of the LSF test cell is also visible during the cooling season, although with a milder magnitude. Once again, the peak values obtained for the insulated configuration assume central importance due to the low magnitude. Considering the ground floor is insulated, the dynamic simulation retrieved a minimum peak value of approximate 5 °C for Bragança, which is around 6 °C lower than the value obtained for the uninsulated configuration.

The annual global variability of indoor air temperatures is in line with the variability of the external weather conditions. The indoor thermal environment of LSF buildings located in climates with higher season variability and more demanding heating and cooling seasons, such as Bragança and Évora, is particularly conditioned by the level of thermal inertia.

Figure 11 presents the annual profiles obtained for the insulated and uninsulated configurations. Similarly to Figure 9, the monthly indoor air temperature amplitude profiles also consider the amplitude of the interquartile range instead of the amplitude of maximum and minimum peak values.

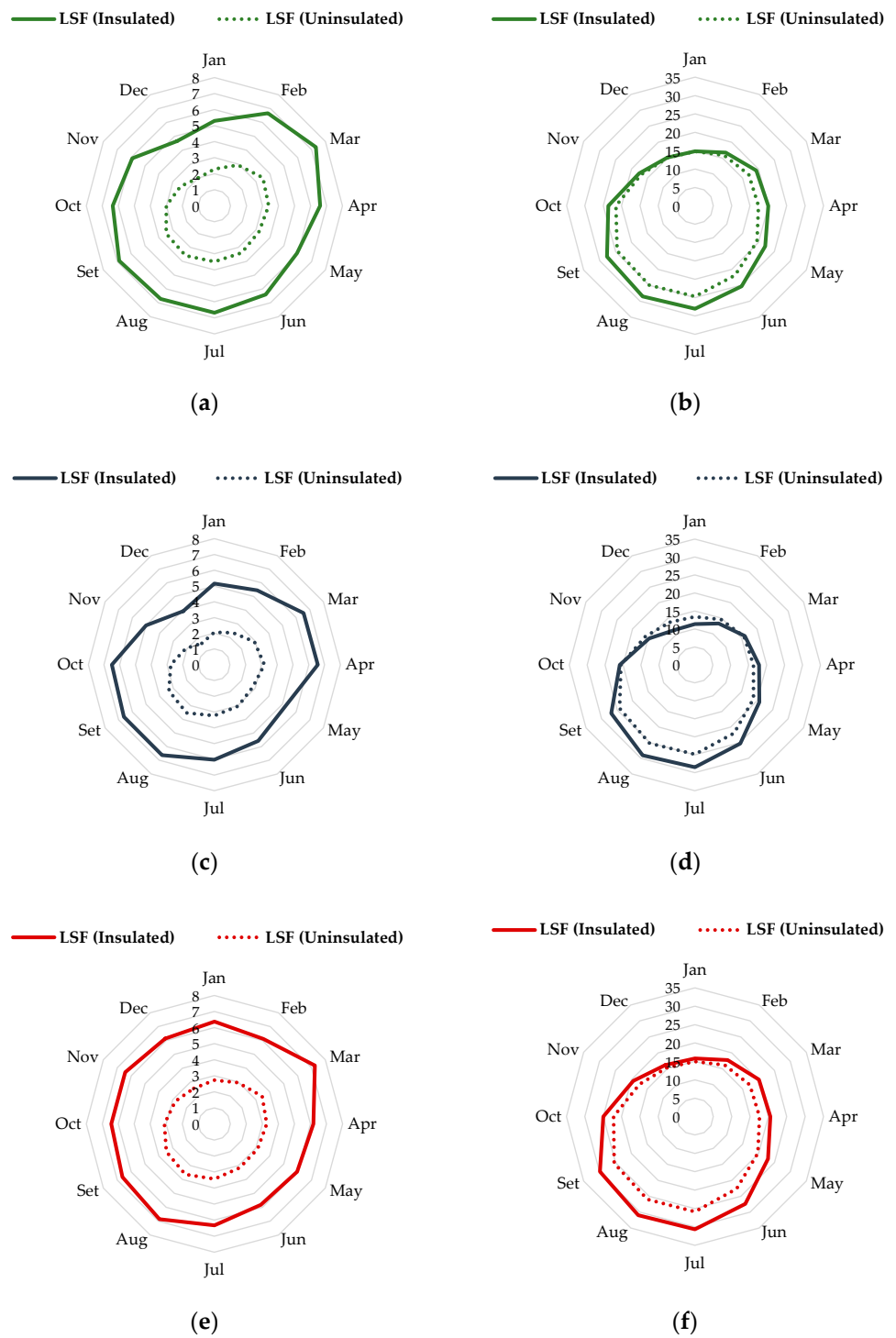
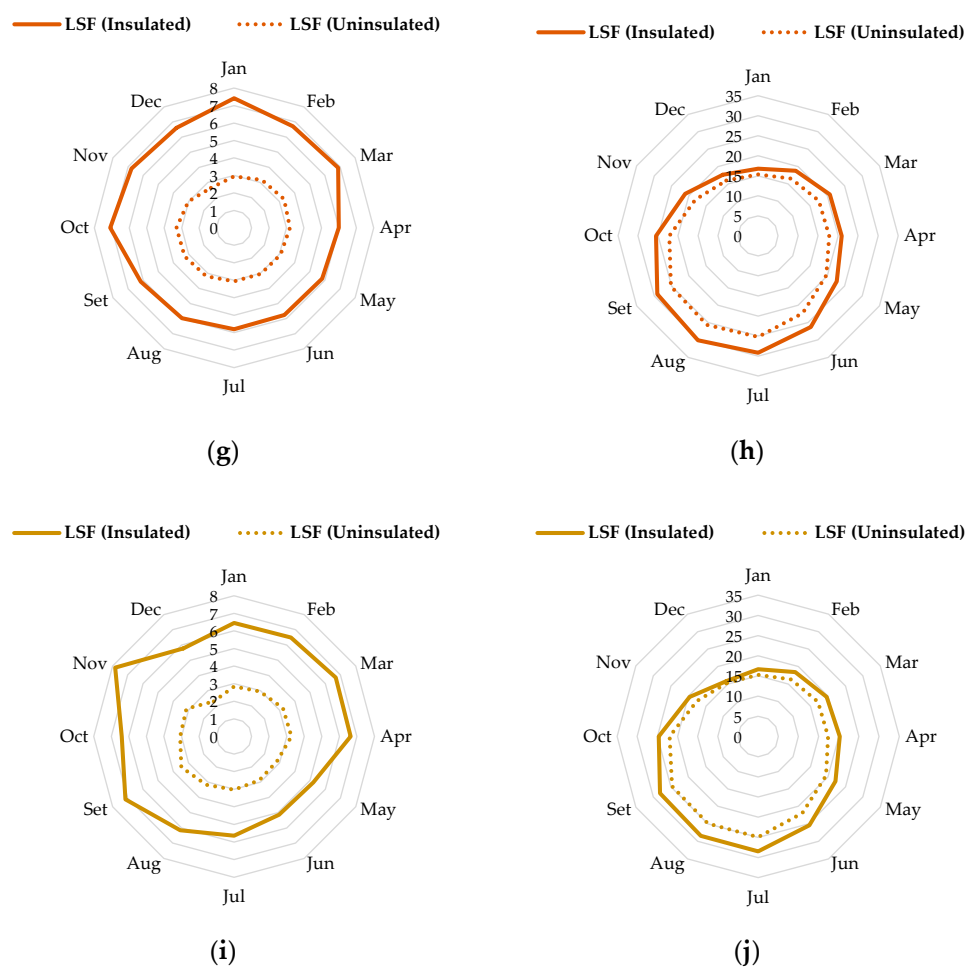


Figure 11. Cont.



**Figure 11.** Monthly indoor air temperature amplitude and median values for the insulated and uninsulated setups obtained from dynamic simulations ( $^{\circ}\text{C}$ ): (a,b) Aveiro; (c,d) Bragança; (e,f) Évora; (g,h) Faro; (i,j) Lisboa.

The analysis of the obtained results in terms of median monthly values, Figure 11b,d,f,h,j, are in line with the conclusions obtained from the analysis of the annual box plot representations in Figure 10. Generally, the median monthly values are superior for the insulated configuration, regardless of the climate conditions. The exception is registered for Bragança, where the median monthly values for the colder months of the heating season (December and January) are inferior for the insulated configuration. This behaviour is due to the more demanding heating season of this climate, as can be observed in Table 1. The further reduced thermal inertia of the insulated configuration leads to a significant indoor air temperature drop during colder periods of winter days, as was observed in Figure 5c, for a milder climate.

On the other hand, it is verified for the remaining four climates that insulating the ground slab allows reaching equivalent or superior values, especially in climates with warmer winters, as Faro. The benefits of insulating the ground slab are supported by the same governing factors previously discussed in the analysis of the representative weeks. Lower thermal inertia enables a greater indoor air temperature buildup during the diurnal period of the winter days, which, in milder climates, may counterbalance the nocturnal temperature drop.

It is during the warmer months of the cooling season when the monthly median values of the two constructive configurations differ, reaching maximum values around  $5^{\circ}\text{C}$  for all the analysed climates. The magnitude of the median values obtained for the insulated configuration during the summer months, surpassing  $30^{\circ}\text{C}$ , highlights the increased



potential for overheating in LSF buildings and the importance of introducing constructive elements capable of offering a robust contribution to the overall thermal inertia.

Figure 11a,c,e,g,i present the average monthly indoor air temperature amplitude value for the insulated and uninsulated configurations. The registered differences continue to show that further reducing the thermal inertia of the LSF test cell highly affects the indoor thermal environment in terms of temperature fluctuations and peak values. The monthly values are between 2 °C and 4 °C for the uninsulated configuration, regardless of the climate, and between 4 °C and 8 °C for the insulated configuration.

Concerning the insulated configuration, it is observed from Figure 11 that, in general terms, despite the overheating potential and high fluctuation of the indoor temperature during the warmer months, commented on earlier, the higher monthly temperature amplitudes are not registered during the summer period. Instead, the maximum values are verified for the winter or shoulder season months. The maximum temperature amplitude during the summer period is only verified for Bragança. Insulating the ground slab enhances a closer response of the indoor thermal environment to the external weather conditions. Therefore, it is when the external weather conditions are more wide-ranging that the indoor environment experiences greater monthly temperature amplitudes.

## 5. Conclusions

A long-term monitoring experimental campaign and dynamic simulations were carried out to evaluate and compare the performance of two different construction systems, considering the southern European climatic context and different configurations in terms of thermal inertia.

The indoor air temperature in the HBM test cell is characterised by higher stability, despite the marked daily fluctuation of the outdoor dry-bulb temperature. On the other hand, the LSF test cell reveals a more dependent behaviour in the outdoor dry-bulb temperature variations. The most significant differences between test cells were registered during the representative summer week.

Despite presenting a more volatile indoor thermal environment, the analysis of the representative winter week has revealed that lower thermal inertia may present some benefits during the colder months. A higher indoor temperature was registered from the afternoon to the end of the daily cycle, which may constitute a significant advantage in the case of intermittent residential occupancy.

The annual profile indicated that the indoor air temperature range is substantially different between the two test cells. However, the monthly median values do not assume a marked difference. In fact, for some months of the monitored period, this difference can be neglected.

The impact of insulating the ground slab is considerably higher in the LSF test cell as the indoor air temperature amplitude in this test cell is higher for every month of the year when considering the insulated configuration. On the other hand, insulating the ground slab of the HBM test cell has resulted in a lower impact on the indoor thermal environment.

Results obtained from the dynamic simulations have shown that insulation of the ground slab of the LSF test cells has a major impact on the indoor thermal environment, regardless of the considered climates. Moreover, it was observed that further reducing the thermal inertia of the LSF test cell significantly jeopardises the indoor thermal environment during the summer by raising the risk and magnitude of overheating, which is particularly concerning in climates with more demanding summers.

On the other hand, it was shown that insulating the ground slab may offer some degree of benefit during the winter months, as also shown by the data from the representative winter week. The dynamic simulations retrieved a similar or superior indoor air temperature median value for the insulated configuration compared with the uninsulated configuration.

Lastly, it was concluded from the dynamic simulations that despite insulating the ground slab of the LSF test cell having a marked influence on the indoor air tempera-

ture during the summer months, it is during the winter and shoulder season that this configuration leads to higher monthly indoor temperature amplitudes.

The presented work aims to reach long-term value by reinforcing the literature with original experimental data within a context where this information is not ample. The experimental results and the respective interpretation and analysis can be significantly beneficial when confronted with studies in this sphere of research that rely exclusively on computational simulations. Moreover, the presented methodology and discussion can enhance existing research for other experimental works around this thematic.

**Author Contributions:** Conceptualization, E.R., R.V., R.M.S.F.A. and V.M.F.; methodology, E.R., R.V., R.M.S.F.A. and V.M.F.; software, E.R., R.V. and R.M.S.F.A.; validation, E.R., R.V. and R.M.S.F.A.; formal analysis, E.R., R.V. and R.M.S.F.A.; investigation, E.R., R.V. and R.M.S.F.A.; resources, E.R., R.V. and V.M.F.; data curation, E.R., R.V. and R.M.S.F.A.; writing—original draft preparation, E.R. and R.M.S.F.A.; writing—review and editing, R.V. and R.M.S.F.A.; visualization, E.R.; supervision, R.V., R.M.S.F.A. and V.M.F.; project administration, E.R., R.V. and R.M.S.F.A.; funding acquisition, E.R., R.V., R.M.S.F.A. and V.M.F. All authors have read and agreed to the published version of the manuscript.

**Funding:** This research received no external funding.

**Institutional Review Board Statement:** Not applicable.

**Informed Consent Statement:** Not applicable.

**Data Availability Statement:** Not applicable.

**Acknowledgments:** The authors wish to acknowledge the company Perfisa—Fábrica de Perfis Metálicos, S.A. for the continuous support of this research work and the provision of cold-formed steel profiles and other constructive materials involved in the construction of the experimental test cells. The authors also want to express their gratitude to the company Preceram—Indústrias de Construção, S.A. for the provision of the materials used in the construction of the hollow brick masonry experimental test cell.

**Conflicts of Interest:** The authors declare no conflict of interest.

## References

1. World Health Organization, Regional Office for Europe. *Combined or Multiple Exposure to Health Stressors in Indoor Built Environments*; Sarigiannis, D.A., Ed.; World Health Organization, Regional Office for Europe: Copenhagen, Denmark, 2014.
2. Yao, Y.; Lian, Z.; Liu, W.; Shen, Q. Experimental study on physiological responses and thermal comfort under various ambient temperatures. *Physiol. Behav.* **2007**, *93*, 310–321. [[CrossRef](#)] [[PubMed](#)]
3. Liu, H.; Li, B.; Chen, L.; Chen, L.; Wu, J.; Zheng, J.; Li, W.; Yao, R. Impacts of Indoor Temperature and Velocity on Human Physiology in Hot Summer and Cold Winter Climate in China. In *Proceedings of the Clima 2007 WellBeing Indoors*, Helsinki, Finland, 10–14 June 2007; FINVAC: Helsinki, Finland, 2007.
4. Kaushik, A.; Arif, M.; Tumula, P.; Ebohon, O.J. Effect of thermal comfort on occupant productivity in office buildings: Response surface analysis. *Build. Environ.* **2020**, *180*, 107021. [[CrossRef](#)]
5. Lan, L.; Wargocki, P.; Lian, Z. Quantitative measurement of productivity loss due to thermal discomfort. *Energy Build.* **2011**, *43*, 1057–1062. [[CrossRef](#)]
6. Ormandy, D.; Ezzratty, V. Health and thermal comfort: From WHO guidance to housing strategies. *Energy Policy* **2012**, *49*, 116–121. [[CrossRef](#)]
7. Sookchaiya, T.; Monyakul, V.; Thepa, S. Assessment of the thermal environment effects on human comfort and health for the development of novel air conditioning system in tropical regions. *Energy Build.* **2010**, *42*, 1692–1702. [[CrossRef](#)]
8. Hawila, A.A.W.; Merabtine, A. A statistical-based optimization method to integrate thermal comfort in the design of low energy consumption building. *J. Build. Eng.* **2021**, *33*, 101661. [[CrossRef](#)]
9. Ferreira, P.; Ruano, A.; Silva, S.; Conceição, E. Neural networks based predictive control for thermal comfort and energy savings in public buildings. *Energy Build.* **2012**, *55*, 238–251. [[CrossRef](#)]
10. Evola, G.; Marletta, L.; Natarajan, S.; Patané, E.M. Thermal inertia of heavyweight traditional buildings: Experimental measurements and simulated scenarios. *Energy Procedia* **2017**, *133*, 42–52. [[CrossRef](#)]
11. Bhamare, D.K.; Rathod, M.K.; Banerjee, J. Passive cooling techniques for building and their applicability in different climatic zones—The state of art. *Energy Build.* **2019**, *198*, 467–490. [[CrossRef](#)]
12. Verbeke, S.; Audenaert, A. Thermal inertia in buildings: A review of impacts across climate and building use. *Renew. Sustain. Energy Rev.* **2018**, *82*, 2300–2318. [[CrossRef](#)]
13. Stazi, F. *Thermal Inertia in Energy Efficient Building Envelopes*; Butterworth-Heinemann: Oxford, UK, 2017; ISBN 9780128139707.

14. Stazi, F.; Tomassoni, E.; Bonfigli, C.; Di Perna, C. Energy, comfort and environmental assessment of different building envelope techniques in a Mediterranean climate with a hot dry summer. *Appl. Energy* **2014**, *134*, 176–196. [[CrossRef](#)]
15. Tonelli, C.; Grimaudo, M. Timber buildings and thermal inertia: Open scientific problems for summer behavior in Mediterranean climate. *Energy Build.* **2014**, *83*, 89–95. [[CrossRef](#)]
16. Roque, E.; Vicente, R.; Almeida, R.M.; Ferreira, V.M. Energy consumption in intermittently heated residential buildings: Light Steel Framing vs hollow brick masonry constructive system. *J. Build. Eng.* **2021**, *43*, 103024. [[CrossRef](#)]
17. Rodrigues, L.T.; Gillott, M.; Tetlow, D. Summer overheating potential in a low-energy steel frame house in future climate scenarios. *Sustain. Cities Soc.* **2013**, *7*, 1–15. [[CrossRef](#)]
18. Hoes, P.; Trcka, M.; Hensen, J.L.M.; Bonnema, B.H. Investigating the potential of a novel low-energy house concept with hybrid adaptable thermal storage. *Energy Convers. Manag.* **2011**, *52*, 2442–2447. [[CrossRef](#)]
19. Evola, G.; Marletta, L. The Effectiveness of PCM Wallboards for the Energy Refurbishment of Lightweight Buildings. *Energy Procedia* **2014**, *62*, 13–21. [[CrossRef](#)]
20. Roque, E.; Santos, P. The Effectiveness of Thermal Insulation in Lightweight Steel-Framed Walls with Respect to Its Position. *Buildings* **2017**, *7*, 13. [[CrossRef](#)]
21. Roque, E.; Santos, P.; Pereira, A. Thermal and Sound Insulation of Lightweight Steel Framed Façade Walls. *Sci. Technol. Built Environ.* **2018**, *25*, 156–176. [[CrossRef](#)]
22. Dubina, D.; Ungureanu, V.; Landolfo, R. *Design of Cold-Formed Steel Structures*; European Convention for Constructional Steelwork (ECCS): Bruxelles, Belgium, 2012; ISBN 978-9-29-147107-2.
23. Santos, P.; Simões da Silva, L.; Ungureanu, V. *Energy Efficiency of Light-Weight Steel-Framed Buildings*; European Convention for Constructional Steelwork (ECCS): Bruxelles, Belgium, 2012; ISBN 978-9-29-147105-8.
24. Burstand, H. *Light Gauge Steel Framing for Housing*; SBI—Swedish Institute of Steel Construction, Publication 170: Stockholm, Sweden, 2000.
25. Samani, P.; Leal, V.; Mendes, A.; Correia, N. Comparison of passive cooling techniques in improving thermal comfort of occupants of a pre-fabricated building. *Energy Build.* **2016**, *120*, 30–44. [[CrossRef](#)]
26. Nawalany, G.; Sokołowski, P. Building–Soil Thermal Interaction: A Case Study. *Energies* **2019**, *12*, 2922. [[CrossRef](#)]
27. Sokołowski, P.; Nawalany, G. Analysis of Energy Exchange with the Ground in a Two-Chamber Vegetable Cold Store, Assuming Different Lengths of Technological Break, with the Use of a Numerical Calculation Method—A Case Study. *Energies* **2020**, *13*, 4970. [[CrossRef](#)]
28. Roque, E.; Vicente, R.; Almeida, R.M.S.F. Indoor Thermal Environment Challenges of Light Steel Framing in the Southern European Context. *Energies* **2021**, *14*, 7025. [[CrossRef](#)]
29. Roque, E.; Vicente, R.; Almeida, R.M. Opportunities of Light Steel Framing towards thermal comfort in southern European climates: Long-term monitoring and comparison with the heavyweight construction. *Build. Environ.* **2021**, *200*, 107937. [[CrossRef](#)]
30. DesignBuilder@. DesignBuilder Software Version 7. London, UK. 2022. Available online: <https://designbuilder.co.uk/> (accessed on 1 April 2022).
31. Direcção Geral de Energia e Geologia (DGEG)@. Lisbon, Portugal. 2022. Available online: <https://www.dgeg.gov.pt/pt/areas-setoriais/energia/eficiencia-energetica/ambiente-e-clima/> (accessed on 1 April 2022).
32. Despacho n.º 15793-F/2013 de 03 de Dezembro do Ministério do Ambiente, Ordenamento de Território e Energia, 35088-(26)-35088(31); Diário da República: Lisboa, Portugal, 2013.
33. ISO 7726:1998; Ergonomics of the Thermal Environment—Instruments for Measuring Physical Quantities. International Organization for Standardization: Geneva, Switzerland, 2015.